

# Tunable and robust room-temperature magnon-magnon entanglement

Yuefei Liu,<sup>1,\*</sup> Andrey Bagrov,<sup>2</sup> Anders Bergman,<sup>3</sup> Anna Delin,<sup>1,4</sup> Olle Eriksson,<sup>3,5</sup> Manuel Pereiro,<sup>3</sup> Simon Streib,<sup>3</sup> Danny Thonig,<sup>5,3</sup> Erik Sjöqvist,<sup>3</sup> and Vahid Azimi-Mousolou<sup>6,3</sup>

<sup>1</sup>*Department of Applied Physics, School of Engineering Sciences,  
KTH Royal Institute of Technology, AlbaNova University Center, SE-10691 Stockholm, Sweden*

<sup>2</sup>*Institute for Molecules and Materials, Radboud University,  
Heyendaalseweg 135, 6525AJ Nijmegen, The Netherlands*

<sup>3</sup>*Department of Physics and Astronomy, Uppsala University, Box 516, SE-751 20 Uppsala, Sweden*

<sup>4</sup>*Swedish e-Science Research Center (SeRC), KTH Royal Institute of Technology, SE-10044 Stockholm, Sweden*

<sup>5</sup>*School of Science and Technology, Örebro University, SE-701 82, Örebro, Sweden*

<sup>6</sup>*Department of Applied Mathematics and Computer Science,  
Faculty of Mathematics and Statistics, University of Isfahan, Isfahan 81746-73441, Iran*

(Dated: September 5, 2022)

Although challenging, realizing controllable high-temperature entanglement is of immense importance for practical applications as well as for fundamental research in quantum technologies. Here, we report the existence of entangled steady states in bipartite quantum magnonic systems at high temperatures. We consider dissipative dynamics of two magnons in a bipartite antiferromagnet or ferrimagnet subjected to a vibrational phonon mode and an external rotating magnetic field. To quantify the bipartite magnon-magnon entanglement, we use the entanglement negativity and compute its dependence on the temperature and magnetic field. We show that, for any given phonon frequency and magnon-phonon coupling rates, there are always ranges of the magnetic field amplitudes and frequencies, for which bipartite magnon-magnon entanglement persists up to and above the room temperature. The generality of the result allows for experimental observation in a variety of crystals and synthetic bipartite antiferromagnetic and ferrimagnetic materials.

Entanglement is a central concept of quantum physics that has developed into a key resource of quantum technology. It makes possible quantum information processing, opens a way towards intercept-resilient quantum communications, and enables increased sensitivity in quantum metrology. If it were possible to overcome the thermal noise and prepare robust entangled quantum states at ambient conditions, the corresponding implications for the future quantum devices would be nearly boundless [1–8]. Recently, quantum computers based on photonics have been demonstrated to achieve quantum advantage at room temperature [5, 6]. Despite this particular success, exploring the potential of other platforms is imperative for the further progress in quantum information processing. Among other options, quantum magnonics exhibits excellent quantum properties over a wide range of temperatures and offers a great opportunity to access pronounced quantum phenomena at room temperature [9, 10]. Compatibility of magnonics with hybrid quantum platforms [9, 11, 12] adds to the advantages of utilizing magnons for quantum data processing.

Most recently, particular attention has been paid to antiferromagnetic quantum magnonics due to its remarkable features including very large equilibrium squeezing and entanglement [13–19]. These properties combined with the thermal stability would allow producing macroscopic quantum entangled states, which are, among other things, particularly important for biomedical applications [20] such as entanglement-enhanced magnetic resonance imaging probes.

Despite the great progress in the field, high-temperature magnon entanglement is yet to be experimentally observed. Here, we report theoretical demonstration of equilibrium magnon-magnon entanglement in bipartite antiferromag-

netic/ferrimagnetic materials. We compute entanglement negativity of a pair of magnon modes coupled to lattice vibrations in the presence of an external rotating magnetic field. We obtain a stationary entanglement diagram in the temperature and magnetic field plane, which clearly shows the possibility of having robust magnon-magnon entanglement above room temperature (Fig. 1). We analyze the magnon entanglement stability against dissipation caused by the spin-lattice magnomechanical interactions and observe that the two-mode magnon system indeed permits high-temperature entanglement at any value of the magnetic field provided that the magnetic field frequency is adjusted to the proper range. This exceptional thermal stability synergizes with other properties distinct from those of photonic platforms such as the equilibrium nature of magnon-magnon entanglement and squeezing, as well as the low magnetic susceptibility of antiferromagnetic materials, which is beneficial for nanoscale miniaturization and higher order of scalability. Altogether, not only this confirms magnonics to be an appropriate complement to the quantum photonic technologies but also opens an avenue to use it as a standalone paradigm that can considerably advance quantum information processing power. In turn, the broad range of crystalline and synthetic antiferromagnetic/ferrimagnetic materials, such as NiO, 2D Ising systems like MnPSe<sub>3</sub>, and YIG-based synthetic antiferromagnets (SAFs)[21–26], provide a space for experimental observation of high-temperature magnon-magnon entanglement.

To pursue our analysis, we assume a bipartite antiferromagnetic material (AFM) subjected to a vibrational mode in a rotating magnetic field as shown in Fig. 2. Through the bosonization procedure, one can describe two sublattices of the bipartite AFM as a pair of magnon modes [13, 16–

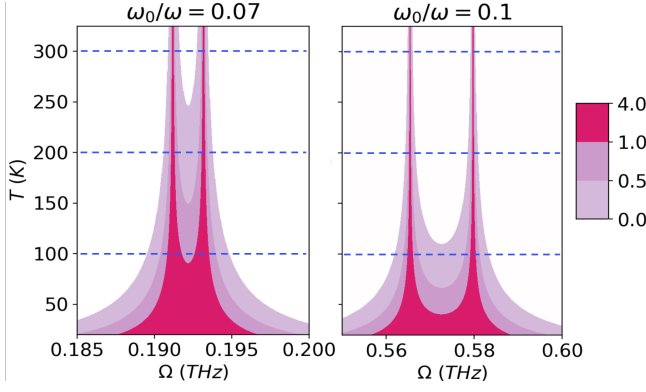


FIG. 1. (Color online) Magnon-magnon entanglement  $E_N$  as a function of the frequency  $\Omega = \mu B_0/\hbar$  associated with the strength  $B_0$  of the rotating magnetic field and the temperature  $T$ . The color bar displays a qualitative illustration of the entanglement, where the white area indicates the separable zone while the red colored zone shows maximum entanglement region in the  $\Omega - T$  plane. Double peaks are associated with the degeneracy of two polarized magnons in antiferromagnetic systems, which is broken in the presence of non-zero magnetic field frequency  $\omega_0$ . The gap between the peaks is proportional to the frequency difference of the two magnons. The frequency ratio  $\omega_0/\omega$  with respect to the magnon frequency at the degeneracy point, i.e.,  $\omega$ , allows one to control the magnon-magnon entanglement region in the  $\Omega - T$  parameter space. The lower the frequency ratio  $\omega_0/\omega$ , the weaker the external magnetic field required to achieve high entanglement at a given temperature (see also Fig. 3). Here, the remaining parameters of the Hamiltonian in Eq. (1) satisfy  $\omega_c/\omega = 1$  and  $g_{ac}/g_{ab} = g_{bc}/g_{ab} = 0.001$ .

18]. The vibrational mode, which may be understood as a mechanical phonon mode below, can couple to the magnon modes through the magnetostrictive force [12]. In the rotating frame, the minimal Hamiltonian of a magnetomechanical system possessing all the aforementioned properties then reads

$$\hat{H} = \hat{H}_0 + \hat{H}_z + \hat{H}_{m-m} + \hat{H}_{m-ph}$$

with

$$\begin{aligned} \hat{H}_0 &= \hbar\omega_a\hat{a}^\dagger\hat{a} + \hbar\omega_b\hat{b}^\dagger\hat{b} + \hbar\omega_c\hat{c}^\dagger\hat{c}, \\ \hat{H}_z &= \hbar\Omega(\hat{a} + \hat{a}^\dagger) + \hbar\Omega(\hat{b} + \hat{b}^\dagger), \\ \hat{H}_{m-m} &= \hbar g_{ab}^*\hat{a}^\dagger\hat{b}^\dagger + \hbar g_{ab}\hat{a}\hat{b}, \\ \hat{H}_{m-ph} &= \hbar\left[g_{ac}\hat{a}^\dagger\hat{a} + g_{bc}\hat{b}^\dagger\hat{b}\right]\left(\frac{\hat{c} + \hat{c}^\dagger}{\sqrt{2}}\right). \end{aligned} \quad (1)$$

Here,  $\hat{a}$  ( $\hat{a}^\dagger$ ),  $\hat{b}$  ( $\hat{b}^\dagger$ ) and  $\hat{c}$  ( $\hat{c}^\dagger$ ) are annihilation (creation) operators of the two AFM magnon modes and the phonon mode, respectively.  $\hat{H}_0$  is their kinetic term with  $\omega_a$ ,  $\omega_b$ ,  $\omega_c$  being the magnon frequencies of the A and B modes, and the phonon frequency, respectively. For simplicity, we assume that the two magnon modes are originally degenerate and have the same frequency  $\omega$ , and the degeneracy is then lifted by the external rotating magnetic field with frequency  $\omega_0$ :  $\omega_a = \omega - \omega_0$ ,  $\omega_b = \omega + \omega_0$ . The Zeemann term  $\hat{H}_z$  describes the interaction between the AFM spin lattice and the magnetic field that rotates in the  $xy$  plane,  $\mathbf{B} = B_0(\cos(\omega_0 t + \theta_0), \sin(\omega_0 t + \theta_0), 0)$ .

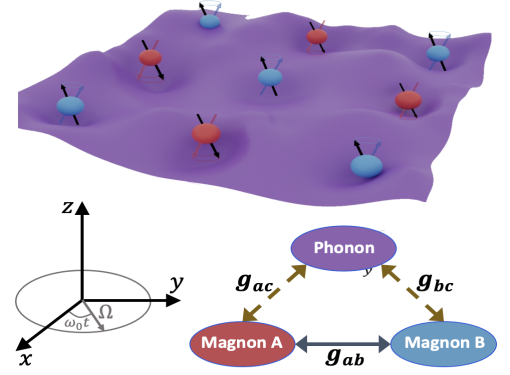


FIG. 2. (Color online) Schematic illustration of bipartite collective spin waves in an antiferromagnetic material subjected to a vibration mechanical phonon mode in a rotating magnetic field.

Without loss of generality, in what follows we take  $\theta_0 = 0$  and absorb the spin magnetic moment into the strength of the external magnetic field:  $\Omega = \mu B_0/\hbar$ . The last two terms define the mutual magnon-magnon interaction [16, 17] and the magnon-phonon interaction with coupling parameters  $g_{ab}$ ,  $g_{ac}$ , and  $g_{bc}$ .

Our main goal is to analyze the robustness of entanglement in the system under dissipation caused by thermal fluctuations, uncontrolled coupling to other internal and external modes, and the related damping in various degrees of freedom and Brownian vibrations. Such dissipative dynamics can be described by nonlinear quantum Langevin equations (QLEs) [27], which in terms of dimensionless quadratures take the form

$$\begin{aligned} \dot{\hat{X}} &= -\kappa_a\hat{X} + \omega_a\hat{Y} - \text{Im}(g_{ab})\hat{x} - \text{Re}(g_{ab})\hat{y} + g_{ac}\hat{Y}\hat{q} \\ &\quad + \sqrt{2}\Omega + \hat{X}^{in}, \\ \dot{\hat{Y}} &= -\omega_a\hat{X} - \kappa_a\hat{Y} - \text{Re}(g_{ab})\hat{x} + \text{Im}(g_{ab})\hat{y} - g_{ac}\hat{X}\hat{q} + \hat{Y}^{in\dagger}, \\ \dot{\hat{x}} &= -\text{Im}(g_{ab})\hat{X} - \text{Re}(g_{ab})\hat{Y} - \kappa_b\hat{x} + \omega_b\hat{y} + g_{bc}\hat{y}\hat{q} \\ &\quad + \sqrt{2}\Omega + \hat{x}^{in}, \\ \dot{\hat{y}} &= -\text{Re}(g_{ab})\hat{X} + \text{Im}(g_{ab})\hat{Y} - \omega_b\hat{x} - \kappa_a\hat{y} - g_{bc}\hat{x}\hat{q} + \hat{y}^{in\dagger}, \\ \dot{\hat{q}} &= \omega_c\hat{p}, \\ \dot{\hat{p}} &= -\frac{g_{ac}}{2}(\hat{X}^2 + \hat{Y}^2 - 1) - \frac{g_{bc}}{2}(\hat{x}^2 + \hat{y}^2 - 1) - \omega_c\hat{q} - \gamma_c\hat{p} + \xi. \end{aligned} \quad (2)$$

We make a connection between the parameters of the Hamiltonian in Eq. (1) and the dimensionless parameters in Eq. (2) in the remark [28].

We show that it is possible to maintain stable magnon-magnon entanglement in an equilibrium setting. Thus, we focus on the steady-state regime, where  $\frac{d}{dt}\langle\hat{O}\rangle = 0$  for  $\hat{O} = \hat{X}, \hat{Y}, \hat{x}, \hat{y}, \hat{p}, \hat{q}$ . Any operator can then be written as a steady-state expectation value plus an additional quantum fluctuation term,  $\hat{O} = \langle\hat{O}\rangle + \delta\hat{O}(t)$  [30]. Imposing the steady-state conditions on Eq. (2) and retaining fluctuations up to linear order, we obtain a set of linear QLEs

$$\dot{u}(t) = Au(t) + n(t), \quad (3)$$

where  $u(t) = (\delta\hat{X}, \delta\hat{Y}, \delta\hat{x}, \delta\hat{y}, \delta\hat{q}, \delta\hat{p})^T$  and  $n(t) = (X^{in}, Y^{in}, x^{in}, y^{in}, 0, \xi)^T$ . Information about steady-state values and coupling constants is encoded in the drift matrix:

$$A = \begin{bmatrix} -\kappa_a & \Delta_{ac} & -\text{Im}(g_{ab}) & -\text{Re}(g_{ab}) & M_Y & 0 \\ -\Delta_{ac} & -\kappa_a & -\text{Re}(g_{ab}) & \text{Im}(g_{ab}) & -M_X & 0 \\ -\text{Im}(g_{ab}) & -\text{Re}(g_{ab}) & -\kappa_b & \Delta_{bc} & M_Y & 0 \\ -\text{Re}(g_{ab}) & \text{Im}(g_{ab}) & -\Delta_{bc} & -\kappa_b & -M_X & 0 \\ 0 & 0 & 0 & 0 & 0 & \omega_p \\ -M_X & -M_Y & -M_X & -M_Y & -\omega_p & -\gamma_p \end{bmatrix}. \quad (4)$$

Here,  $\Delta_{ac} = \omega_a + g_{ac}\langle\hat{q}\rangle$  and  $\Delta_{bc} = \omega_b + g_{bc}\langle\hat{q}\rangle$  are the effective magnon frequency detunings induced by the magnon-phonon interaction. The effective magnon-phonon couplings for both magnon modes are given by  $M_X = g_{ac}\langle\hat{X}\rangle$ ,  $M_Y = g_{ac}\langle\hat{Y}\rangle$ , and  $M_x = g_{bc}\langle\hat{x}\rangle$ ,  $M_y = g_{bc}\langle\hat{y}\rangle$ . Assuming low dissipation of the magnon modes in typical AFM structures [39, 40],  $\kappa_a, \kappa_b \ll \Delta_{ac}, \Delta_{bc}$ , we obtain the steady-state solutions as

$$\begin{aligned} \langle X \rangle &= \frac{\sqrt{2}\Omega \text{Im}(g_{ab})}{\Delta_{ac}\Delta_{bc} - |g_{ab}|^2}, \quad \langle Y \rangle = \frac{-\sqrt{2}\Omega [\Delta_{bc} + \text{Re}(g_{ab})]}{\Delta_{ac}\Delta_{bc} - |g_{ab}|^2}, \\ \langle x \rangle &= \frac{\sqrt{2}\Omega \text{Im}(g_{ab})}{\Delta_{ac}\Delta_{bc} - |g_{ab}|^2}, \quad \langle y \rangle = \frac{-\sqrt{2}\Omega [\Delta_{ac} + \text{Re}(g_{ab})]}{\Delta_{ac}\Delta_{bc} - |g_{ab}|^2}, \\ \frac{\omega_p}{\Omega^2} \langle q \rangle + \frac{g_{ac}(\Delta_{bc} + g_{ab})^2 + g_{bc}(\Delta_{ac} + g_{ab})^2}{(\Delta_{ac}\Delta_{bc} - |g_{ab}|^2)^2} &= 0. \end{aligned} \quad (5)$$

Once the frequencies and exchange parameters are set as parameters of the model Hamiltonian by Eq. (1), the explicit form of the drift matrix  $A$  mainly depends on the steady-state value of  $\langle\hat{q}\rangle$ , which is given as a root of the polynomial of degree five specified by the last algebraic equation in Eq. (5). As a frequency shift in magnon modes, only the real-valued roots of  $\langle\hat{q}\rangle$  are physically meaningful.

The linear form of QLEs in Eq. (3) ensures that the dynamics of quantum fluctuations is Gaussian and can be completely characterized by the corresponding covariance correlation matrix (CCM) [31]. Using the fact that different components of the input noise vector  $n(t)$  are uncorrelated, the steady-state CCM denoted by  $V$  can be obtained through the Lyapunov equation [21, 29]

$$A \cdot V + V \cdot A^* = -D \quad (6)$$

where  $D = \text{Diag}[\kappa_a(2N_a+1), \kappa_a(2N_a+1), \kappa_b(2N_b+1), \kappa_b(2N_b+1), 0, \gamma_p(2N_p+1)]$  is the diffusion matrix. Solving Eq. (6) for  $V$ , one can evaluate the bipartite magnon-magnon entanglement by computing the logarithmic negativity for two-mode Gaussian states defined as [21, 31, 32]

$$E_N \equiv \max[0, -\ln(2\tilde{v}_-)], \quad (7)$$

where  $\tilde{v}_-$  is the minimum symplectic eigenvalue of  $V_4$ , being the  $4 \times 4$  reduced CCM obtained by projecting  $V$  onto the two magnon modes. This eigenvalue can be computed as  $\tilde{v}_- = \min \text{eig}[i\Upsilon\tilde{V}_4]$ , for the symplectic matrix  $\Upsilon = \oplus_{j=1}^2 i\sigma_y$  (with  $\sigma_y$  being the Pauli-y matrix) and the partial transpose  $\tilde{V}_4 = P_{1|2}V_4P_{1|2}$  with  $P_{1|2} = \text{diag}(1, -1, 1, 1)$ .

The magnon-magnon logarithmic negativity in the steady-state limit as a function of the external magnetic field and temperature is shown in Fig. 1. As can be seen, our analysis reveals magnon-magnon entanglement up to and above room temperature. For any given rotation frequency of the magnetic field  $\omega_0$ , there always exists a certain range of the field amplitudes  $\Omega$ , where magnon-magnon entanglement can be realized at a high temperature. Moreover, the entangled region including the high-temperature entanglement zone in the  $\Omega - T$  parameter space can be efficiently placed around practically feasible parameter values by controlling the frequency ratio  $\omega_0/\omega$ , i.e., the ratio between the rotation frequency of the external magnetic field and the magnon frequency  $\omega$  at the degeneracy point of  $\omega_0 = 0$ . In other words, magnon-magnon entanglement can be realized for any positive value of  $\Omega$  at a given temperature  $T$  if the frequency ratio  $\omega_0/\omega$  is properly adjusted. To further elaborate on this, in Fig. 3 we show how some cuts of the entangled region in Fig. 1 at three different temperatures move along the parameter domain of  $\Omega$  upon varying the control parameter  $\omega_0/\omega$ .

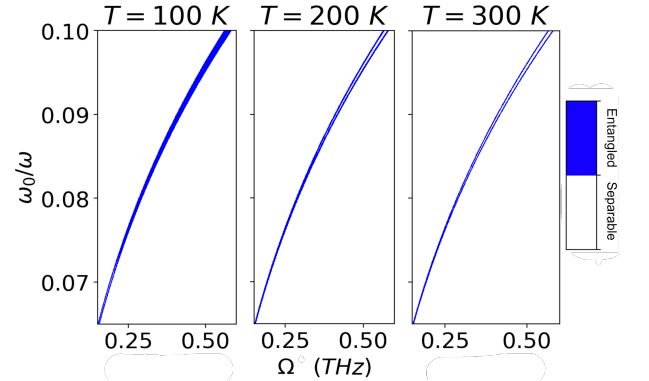


FIG. 3. (Color online) Magnon-magnon entanglement  $E_N$  as a function of the frequency ratio  $\omega_0/\omega$  and external magnetic field strength  $\Omega$  at three temperatures  $T = 100$  K (left),  $T = 200$  K (middle) and  $T = 300$  K (right). The dark blue color specifies non-zero entanglement. We keep  $g_{ac}/g_{ab} = g_{bc}/g_{ab} = 0.001$  and  $\omega_c/\omega = 1$  the same as the parameter values used for Fig. 1.

Figures 1 and 3 are plotted for fixed values of the phonon frequency  $\omega_c$  and magnon-phonon couplings  $g_{ac}$  and  $g_{bc}$ . In a search for a real material that can serve as an optimal host for robustly entangled magnon modes, it is instructive to also understand the dependence of entanglement on these material parameters. This is shown in Fig. 4 and 5. One can see that, in a wide range of couplings and phonon frequencies, it is possible to have non-zero entanglement at rather large (and even ambient) temperatures if frequency and amplitude of the rotating magnetic field are tuned to proper values. Fig. 4 demonstrates that for any given magnon-phonon coupling  $g_{ac} = g_{bc}$ , there always exists a narrow window of phonon frequencies, where the same magnon-magnon entanglement as shown in the Fig. 1 occurs.

We further examine the effect of asymmetric magnon-phonon couplings on the magnon-magnon entanglement re-

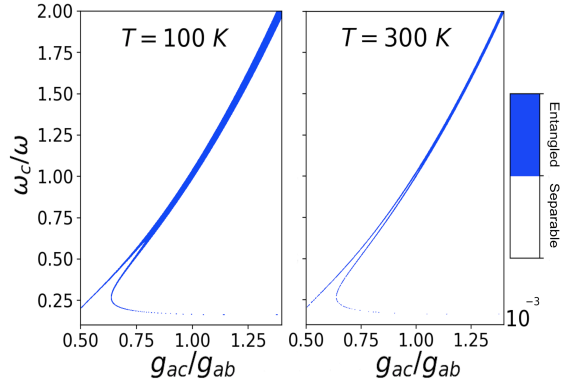


FIG. 4. (Color online) The range of phonon-magnon frequency ratio, which allows the same magnon-magnon entanglement pattern in Fig. 1, as a function of magnon-phonon coupling ratios  $g_{ac}/g_{ab}$ . Note that we have assumed  $g_{ac}/g_{ab} = g_{bc}/g_{ab}$  here. Although the plots corresponds to the non-zero magnon-magnon entanglement at  $\Omega = 0.1932$  THz,  $\omega_0/\omega = 0.07$  and temperatures  $T = 100$  K (left) and  $T = 300$  K (right), similar ranges of phonon-magnon frequency ratios appear at other points of the entanglement diagram in Fig. 1. The higher the temperature the narrower the range of relative phonon frequency.

gion in Fig. 1. For a frequency  $\omega_c$ , Fig. 5 illustrates the wide range of different coupling strengths  $g_{ac} \neq g_{bc}$ , which allows the same entanglement diagram as in Fig. 1. Fig. 5 shows that, even up to high temperatures about  $T = 300$  K, for different values of coupling rates varying in a wide range, there is a value of phonon frequency  $\omega_c/\omega$  that guarantees non-zero magnon-magnon entanglement. Besides, it implies that a broad family of bipartite ferrimagnetic materials are likely to have a similar magnon-magnon entanglement diagram, as shown in Fig. 1.

To observe the high-temperature magnon-magnon entanglement experimentally, one can use the setting based on coupling the magnons to a microwave cavity, as proposed in [17]. From the performed analysis, one can conclude that, in order to host considerable magnon-magnon entanglement, the AFM material should have a large characteristic phonon frequency and relatively strong magnon-phonon coupling. Besides keeping in mind that, to find a suitable material, it is mandatory to take into account such properties as the Néel temperature, magnon damping rate, and gyromagnetic ratio, which would have an impact on the results outlined above. Among many appropriate classes of compounds, NiO is a concrete example of a crystal AFM [33–36] with high Néel temperature of  $T_N^{\text{NiO}} = 523\text{K}$  and large magnon lifetime set by the low damping rate  $\alpha = (5.0 \pm 0.4) \times 10^{-4}$ . In the case of synthetic AFMs, YIG-based structures have attracted significant attention in magnonics due to their unique properties such as low damping rate  $\alpha = 3 \times 10^{-5}$  and strong magnon-magnon coupling [21, 22, 26, 37, 38]. For the low-lying excitations,  $\langle a^\dagger a \rangle, \langle b^\dagger b \rangle \ll 2Ns$ , where  $N = \rho V$  is the total number of spins in each YIG sublattice and  $s = 5/2$ , the driving field  $\Omega$  is given by  $\Omega = \frac{\sqrt{5}}{4}\gamma\sqrt{N}B_0$ . Here,  $\gamma/2\pi = 28\text{GHz/T}$  is the

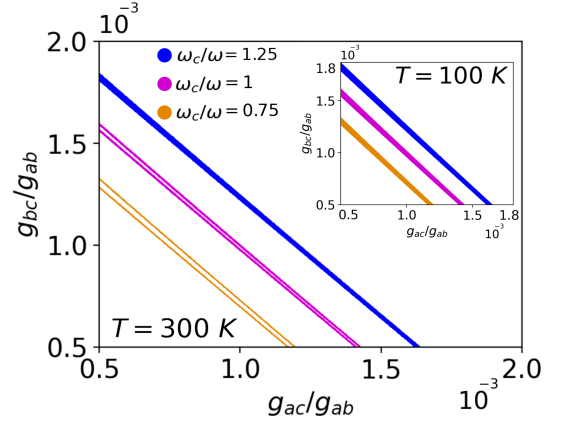


FIG. 5. (Color online) The range of asymmetric magnon-phonon couplings, which allows the same magnon-magnon entanglement pattern in Fig. 1, for a given phonon frequency. The plot corresponds to the non-zero magnon-magnon entanglement at  $\Omega = 0.1932$  THz,  $\omega_0/\omega = 0.07$  and temperature  $T = 300$  K ( $T = 100$  K for inset) for  $\omega_c/\omega = 0.75$  (yellow),  $\omega_c/\omega = 1$  (pink) and  $\omega_c/\omega = 1.25$  (blue). Similar patterns occur for any other point from the entangling diagram in Fig. 1 and any other value of  $\omega_c/\omega$ . The higher the temperature the narrower the range of asymmetric magnon-phonon couplings for a given  $\omega_c/\omega$ .

gyromagnetic ratio,  $\rho = 4.22 \times 10^{27} \text{ m}^{-3}$  is the spin density, and  $V$  is the volume of the YIG sample in each sublattice of the YIG-based synthetic AFM.

In this paper, we have computed bipartite magnon-magnon entanglement quantified by logarithmic negativity in a general setting of a bipartite antiferromagnetic material subjected to thermal noise and an external rotating magnetic field. We have shown that it is possible to observe stable entanglement between magnons of different sublattices. Notably, the entanglement can persist even above room temperature. The high-temperature magnon-magnon entanglement turns out to be quite a general and robust phenomenon, meaning that, for any given material, it can be ensured by tuning the external magnetic field frequency and amplitude in a physically reasonable range of scales. The results presented here are relevant for many classes of compounds that can be studied experimentally. To name a few, NiO and YIG-based synthetic antiferromagnets with high Néel temperatures and low damping rates appear to be promising examples. An experimental test of our findings can lead to significant achievements in the emerging field of quantum magnonics and its applications towards the room-temperature quantum technologies.

*Acknowledgments:* The authors acknowledge financial support from the Knut and Alice Wallenberg Foundation through Grant No. 2018.0060. A.B. and O.E. acknowledges eSSSENCE. A.D. acknowledges financial support from the Swedish Research Council (VR) through Grants No. 2019-05304 and 2016-05980. O.E. acknowledges support by the Swedish Research Council (VR), the Foundation for Strategic Research (SSF), the European Research Council (854843-FASTCORR) and STandUP. D.T. acknowledges support from

the Swedish Research Council (VR) with grant No. 2019-03666. Y. L. acknowledges financial support from the KTH-CSC scholarship agreement (No. 201907090094). E.S. acknowledges financial support from the Swedish Research Council (VR) through Grant No. 2017-03832.

---

\* yuefei@kth.se

- [1] F. Galve, L. A. Pachón, and D. Zueco, Bringing Entanglement to the High Temperature Limit, *Phys. Rev. Lett.* **105**, 180501 (2010).
- [2] F. Dolde, I. Jakobi, B. Naydenov, N. Zhao, S. Pezzagna, C. Trautmann, J. Meijer, P. Neumann, F. Jelezko, and J. Wrachtrup, Room-temperature entanglement between single defect spins in diamond, *Nat. Phys.* **9**, 139 (2013).
- [3] F. Wang, Y.-Y. Huang, Z.-Y. Zhang, C. Zu, P.-Y. Hou, X.-X. Yuan, W.-B. Wang, W.-G. Zhang, L. He, X.-Y. Chang, and L.-M. Duan, Room-temperature storage of quantum entanglement using decoherence-free subspace in a solid-state spin system, *Phys. Rev. B* **96**, 134314 (2017).
- [4] Q. Lin, B. He, and M. Xiao, Entangling Two Macroscopic Mechanical Resonators at High Temperature, *Phys. Rev. Appl.* **13**, 034030 (2020).
- [5] H. S. Zhong, H. Wang, Y.-H. Deng, M.-C. Chen, L.-C. Peng, Y.-H. Luo, J. Qin, D. Wu, X. Ding, Y. Hu, P. Hu, X.-Y. Yang, W.-J. Zhang, H. Li, Y. Li, X. Jiang, L. Gan, G. Yang, L. You, Z. Wang, L. Li, N.-L. Liu, C.-Y. Lu, and J.-W. Pan, Quantum computational advantage using photons, *Science* **370**, 1460 (2020).
- [6] J. M. Arrazola, V. Bergholm, K. Brádler, T. R. Bromley, M. J. Collins, I. Dhand, A. Fumagalli, T. Gerrits, A. Goussev, L. G. Helt, J. Hundal, T. Isacsson, R. B. Israel, J. Izaac, S. Jahangiri, R. Janik, N. Killoran, S. P. Kumar, J. Lavoie, A. E. Lita, D. H. Mahler, M. Menotti, B. Morrison, S. W. Nam, L. Neuhaus, H. Y. Qi, N. Quesada, A. Repeatingon, K. K. Sabapathy, M. Schuld, D. Su, J. Swinerton, A. Száva, K. Tan, P. Tan, V. D. Vaidya, Z. Vernon, Z. Zabaneh, and Y. Zhang, Quantum circuits with many photons on a programmable nanophotonic chip, *Nature* **591**, 54 (2021).
- [7] M. Gulka, D. Wirtitsch, V. Ivády, J. Vodnik, J. Hruby, G. Magchiels, E. Bourgeois, A. Gali, M. Trupke, and M. Nesladek, Room-temperature control and electrical readout of individual nitrogen-vacancy nuclear spins, *Nat. Commun.* **12**, 4421 (2021).
- [8] F. D. Bello, N. Kongsuwan, and O. Hess, Near-Field Generation and Control of Ultrafast, Multipartite Entanglement for Quantum Nanoplasmonic Networks, *Nano Lett.* **22**, 2801 (2022).
- [9] H. Y. Yuan, Y. Cao, A. Kamra, R. A. Duine, and P. Yan, Quantum magnonics: when magnon spintronics meets quantum information science, *Phys. Rep.* **965**, 1 (2022).
- [10] A. Barman, G. Gubbiotti, S. Ladak, A. O. Adeyeye, M. Krawczyk, J. Gräfe, C. Adelmann, S. Cotozana, A. Naemi, V. I. Vasyuchka, B. Hillebrands, S. A. Nikitov, H. Yu, D. Grundler, A. V. Sadovnikov, A. A. Grachev, S. E. Sheshukova, J.-Y. Duquesne, M. Marangolo, G. Csaba, W. Porod, V. E. Demidov, S. Urazhdin, S. O. Demokritov, E. Albisetti, D. Petti, R. Bertacco, H. Schultheiss, V. V. Kruglyak, V. D. Poimanov, S. Sahoo, J. Sinha, H. Yang, M. Münzenberg, T. Moriyama, S. Mizukami, P. Landeros, R. A. Gallardo, G. Carloti, J.-V. Kim, R. L. Stamps, R. E. Camley, B. Rana, Y. Otani, W. Yu, T. Yu, G. E. W. Bauer, C. Back, G. S. Uhrig, O. V. Dobrovolskiy, B. Budinska, H. Qin, S. van Dijken, A. V. Chumak, A. Khitun, D. E. Nikonov, I. A. Young, B. W. Zingsem, and M. Winklhofer, The 2021 Magnonics Roadmap, *J. Phys. Condens. Matter* **33**, 413001 (2021).
- [11] Y. Tabuchi, S. Ishino, A. Noguchi, O. Ishikawa, R. Yamazaki, K. Usami, and Y. Nakamura, Quantum magnonics: The magnon meets the superconducting qubit, *C. R. Phys.* **17**, 729 (2016).
- [12] D. Lachance-Quirion, Y. Tabuchi, A. Gloppe, K. Usami, and Y. Nakamura, Hybrid quantum systems based on magnonics, *Appl. Phys. Express* **12**, 070101 (2019).
- [13] D. Bossini, S. Dal Conte, G. Cerullo, O. Gomonay, R. V. Pisarev, M. Borovsak, D. Mihailovic, J. Sinova, J. H. Mentink, Th. Rasing, and A. V. Kimel, Laser-driven quantum magnonics and terahertz dynamics of the order parameter in antiferromagnets, *Phys. Rev. B* **100**, 024428 (2019).
- [14] A. Kamra, E. Thingstad, G. Rastelli, R. A. Duine, A. Brataas, W. Belzig, and A. Sudbø, Antiferromagnetic magnons as highly squeezed Fock states underlying quantum correlations, *Phys. Rev. B* **100**, 174407 (2019).
- [15] H. Y. Yuan, Sh. Zheng, Z. Ficek, Q. Y. He, and M.-H. Yung, Enhancement of magnon-magnon entanglement inside a cavity, *Phys. Rev. B* **101**, 014419 (2020).
- [16] V. Azimi-Mousolou, A. Bagrov, A. Bergman, A. Delin, O. Eriksson, Y. Liu, M. Pereiro, D. Thonig, and E. Sjöqvist, Hierarchy of magnon mode entanglement in antiferromagnets, *Phys. Rev. B* **102**, 224418 (2020).
- [17] V. Azimi-Mousolou, Y. Liu, A. Bergman, A. Delin, O. Eriksson, M. Pereiro, D. Thonig, and E. Sjöqvist, Magnon-magnon entanglement and its quantification via a microwave cavity, *Phys. Rev. B* **104**, 224302 (2021).
- [18] D. Wuhler, N. Rohling, and W. Belzig, Theory of quantum entanglement and structure of the two-mode squeezed antiferromagnetic magnon vacuum, *Phys. Rev. B* **105**, 054406 (2022).
- [19] A. Kamra, W. Belzig, and A. Brataas, Magnon-squeezing as a niche of quantum magnonics, *Appl. Phys. Lett.* **117**, 090501 (2020).
- [20] M. Arndt, T. Juffmann, and V. Vedral, Quantum physics meets biology, *HFSP journal* **3**, 386 (2009).
- [21] J. Li, S.-Y. Zhu and G. S. Agarwal, Magnon-Photon-Phonon Entanglement in Cavity Magnomechanics, *Phys. Rev. Lett.* **121**, 203601 (2018).
- [22] T. Kikkawa, K. Shen, B. Flebus, R. A. Duine, K. Uchida, Z. Qiu, G. E. W. Bauer, and E. Saitoh, Magnon Polarons in the Spin Seebeck Effect, *Phys. Rev. Lett.* **117**, 207203 (2016).
- [23] H. T. Simensen, R. E. Troncoso, A. Kamra, and A. Brataas, Magnon-polarons in cubic collinear antiferromagnets, *Phys. Rev. B* **99**, 064421 (2019).
- [24] T. T. Mai, K. F. Garrity, A. McCreary, J. Argo, J. R. Simpson, V. Doan-Nguyen, R. Valdés Aguilar and A. R. Hight Walker, Magnon-phonon hybridization in 2D antiferromagnet MnPSe<sub>3</sub>, *Sci. Adv.* **9**, eabj3106 (2021).
- [25] S. Liu, A. Granados del Águila, D. Bhowmick, C. Kwan Gan, T. Thu Ha Do, M. A. Prosnikov, D. Sedmidubský, Z. Sofer, P. C. M. Christianen, P. Sengupta, and Q. Xiong, Direct Observation of Magnon-Phonon Strong Coupling in Two-Dimensional Antiferromagnet at High Magnetic Fields, *Phys. Rev. Lett.* **127**, 097401 (2021).
- [26] C. Dai and F. Ma, Strong magnon-magnon coupling in synthetic antiferromagnets, *Appl. Phys. Lett.* **118**, 112405 (2021).
- [27] V. Giovannetti and D. Vitali, Phase-noise measurement in a cavity with a movable mirror undergoing quantum Brownian motion, *Phys. Rev. A* **63**, 023812 (2001).
- [28] It is handy to introduce dimensionless quadratures  $\hat{X} = (\hat{a} +$

- $\hat{a}^\dagger)/\sqrt{2}$ ,  $\hat{Y} = i(\hat{a}^\dagger - \hat{a})/\sqrt{2}$ ,  $\hat{x} = (\hat{b} + \hat{b}^\dagger)/\sqrt{2}$ , and  $\hat{y} = i(\hat{b}^\dagger - \hat{b})/\sqrt{2}$  for the magnon modes  $\hat{a}, \hat{b}$ . For magnons the nonlinear quantum Langevin equations are described by  $\dot{\hat{O}} = \frac{i}{\hbar}[\hat{H}, \hat{O}] - \kappa_o \hat{O} + \sqrt{2\kappa_o} \hat{O}^{in}$ , where  $\kappa_o$  is the dissipation/damping rate, and  $\hat{O}^{in} = (\hat{o}^{in} + \hat{o}^{in\dagger})/\sqrt{2}$  or  $\hat{O}^{in} = i(\hat{o}^{in\dagger} - \hat{o}^{in})/\sqrt{2}$ ,  $\hat{o} = \hat{a}, \hat{b}$ , is the input noise operator associated with the magnon modes  $\hat{O} = \hat{X}, \hat{x}$  or  $\hat{O} = \hat{Y}, \hat{y}$ , respectively. The input noise operators are characterized by the correlation functions  $\langle \hat{o}^{in\dagger}(t) \hat{o}^{in}(t') \rangle = 2\kappa_o N(\omega_o) \delta(t - t')$ ,  $\langle \hat{o}^{in}(t) \hat{o}^{in\dagger}(t') \rangle = 2\kappa_o [N(\omega_o) + 1] \delta(t - t')$ , with the equilibrium thermal mean magnon occupation numbers  $N(\omega_o) = [\exp(\hbar\omega_o/k_B T) - 1]^{-1}$ . In a similar manner we may define  $\hat{q} = (\hat{c} + \hat{c}^\dagger)/\sqrt{2}$ , and  $\hat{p} = i(\hat{c}^\dagger - \hat{c})/\sqrt{2}$  to be the dimensionless quadratures associated with the mechanical phonon mode. A Markovian description of quantum Brownian motion for a mechanical mode with large quality factor  $Q = \omega_c/\gamma_c \gg 1$  is set by  $\dot{\hat{q}} = \frac{i}{\hbar}[\hat{H}, \hat{q}]$ ,  $\dot{\hat{p}} = \frac{i}{\hbar}[\hat{H}, \hat{p}] - \gamma_c \hat{p} + \xi$ , with mechanical damping rate  $\gamma_c$  and input noise operator  $\xi$  given by the correlation function [21, 27, 29]  $\langle \hat{\xi}(t) \hat{\xi}(t') + \hat{\xi}(t') \hat{\xi}(t) \rangle \simeq 2\gamma_c [2N_c(\omega_c) + 1] \delta(t - t')$ , where  $N_c(\omega_c) = [\exp(\hbar\omega_c/k_B T) - 1]^{-1}$  is the equilibrium thermal mean phonon occupation number.
- [29] D. Vitali, S. Gigan, A. Ferreira, H. R. Böhm, P. Tombesi, A. Guerreiro, V. Vedral, A. Zeilinger, and M. Aspelmeyer, Optomechanical Entanglement between a Movable Mirror and a Cavity Fields, *Phys. Rev. Lett.* **98**, 030405 (2007).
- [30] S. Mancini and P. Tombesi, Quantum noise reduction by radiation pressure, *Phys. Rev. A* **49**, 4055 (1994).
- [31] G. Adesso, A. Serafini, and F. Illuminati, Extremal entanglement and mixedness in continuous variable systems, *Phys. Rev. A* **70**, 022318 (2004).
- [32] G. Vidal and R. F. Werner, Computable measure of entanglement, *Phys. Rev. A* **65**, 032314 (2002).
- [33] W. L. Roth, Magnetic Structures of MnO, FeO, CoO, and NiO, *Phys. Rev.* **101**, 1333 (1958).
- [34] T. Moriyama, K. Hayashi, K. Yamada, M. Shima, Y. Ohya, and T. Ono, Intrinsic and extrinsic antiferromagnetic damping in NiO, *Phys. Rev. Mater.* **3**, 051402 (2019).
- [35] J. R. Tomlinson, L. Domash, R. G. Hay, and C. W. Montgomery, The High Temperature Heat Content of Nickel Oxide, *J. Am. Chem. Soc.* **77**, 909 (1955).
- [36] H. Momida, and T. Oguchi, First-Principles Studies of Antiferromagnetic MnO and NiO Surfaces, *J. Phys. Soc. Jpn.* **72**, 588 (2003).
- [37] X. Zhang, C.-L. Zou, L. Jiang, and H. X. Tang, Cavity magnomechanics, *Science Advances* **2**, e1501286 (2016).
- [38] E. G. Spencer, R. C. LeCraw, and A. M. Clogston, Low-temperature line-width maximum in yttrium iron garnet, *Phys. Rev. Lett.* **3**, 32 (1959).
- [39] V. V. Kruglyak, S. O. Demokritov, and D. Grundler, Magnonics, *J. Phys. D: Appl. Phys.* **43**, 260301(2010).
- [40] B. Lenk, H. Ulrichs, F. Garbs, and M. Münzenberg, The building blocks of magnonics, *Phys. Rep.* **507**, 107 (2011).